Mechanism of hysteresis in shock wave reflection

Yan-Chao Hu (胡延超) [1] Wen-Feng Zhou (周文丰) [1,2] Zhi-Gong Tang (唐志共)[3,*]
Yan-Guang Yang (杨彦广) [3,†] and Zhao-Hu Qin (秦兆虎)[2]

[1]*Hypervelocity Aerodynamics Institute, China Aerodynamics Research and Development Centre, Mianyang 621000, China*
[2]*State Key Laboratory for Turbulence and Complex Systems, College of Engineering, Peking University, Beijing 100871, China*
[3]*China Aerodynamics Research and Development Centre, Mianyang 621000, China*

This paper reports on the mechanism of the hysteresis in the transition between regular and Mach shock wave reflections. We disclose that, for a given inflow Mach number, a stable reflection configuration should maintain the minimal dissipation. As the wedge angle varies, the set of the minimal dissipation points forms the valley lines in the dissipation landscape, and these valley lines compose the hysteresis loop. The saddle-nodes, intersections of the ridge line, and the valley lines are actually the transition points. Additionally, the predicted reflection configurations agree well with the experimental and numerical results, validating this theory.

I. INTRODUCTION

Hysteresis is a general property of systems with two or more possible steady states. A canonical example is provided by ferromagnetic systems [1], where the intensity variation of the magnetic field can induce a magnetization hysteresis. Classic hysteresis models [2,3], such as Preisach model [4] for magnetic hysteresis, Bouc-Wen model [5–7] for structural engineering, and dynamical hysteresis model [8] for periodically switched bistable systems, have captured main features of hysteresis, mathematically. In the shock wave reflection system, the hysteresis process also exists and has an important impact on supersonic and hypersonic flight performance [9]. Consequently, shock wave reflection hysteresis (SRH) is of both theoretical value and engineering applications significance. Different from the classic hysteresis models, a geometry method is proposed to describe SRH process in this paper.

In 1878, conducting his experiments in a shock tube, Mach [10] first found two types of shock wave reflection—regular reflections (RR) and Mach reflections (MR), for a given combination of incident shock wave Mach number M_s and wedge angle θ_w. In wind tunnel experiments, for a given inflow Mach number M_0, these two shock reflection configurations can also be observed with θ_w varying. As shown in Fig. 1(a), the presence of a Mach stem—one segment of strong concave shock wave—is the main distinction between RRs (states 1 and 2) and MRs (states 3 and 4); see also Figs. 3(a) and 3(b) for details. Later on, von Neumann [11,12] proposed two critical wedge angles, θ_w^N and θ_w^D, as shown in Figs. 1(b) and 1(c), and clarified that only RRs exist when $\theta_w < \theta_w^N$ (the overall RR domain); only MRs exist when $\theta_w > \theta_w^D$ (the overall MR domain); both stable RRs and MRs are mathematically possible when $\theta_w^N \leqslant \theta_w \leqslant \theta_w^D$ (the dual-solution domain). Based on the possibility two steady states existing in the dual-solution domain, Hornung [13] hypothesized that SRHs could exist in

RRs $\rightleftharpoons$ MRs transitions. Subsequently, the existence of SRHs was verified both experimentally [14–17] and numerically [14,18–20]. Figure 1(a) shows flow configurations of hysteresis induced by θ_w variation for a given $M_0 = 4.5$. As θ_w varies continuously from $20°$ (state 1 in the overall RR domain) to $24°$ (state 2 in the dual-solution domain), the configuration maintains a stable RR. However, if θ_w varies from $28°$ (state 3 in the overall MR domain) back to $24°$ (state 4 in the overall MR domain), then it will maintain a stable MR. Note that whether the reflection configuration at $\theta_w = 24°$ is a stable RR (state 2) or a stable MR (state 4) depends on its evolution history, and states $1 \rightarrow 2 \rightarrow 3 \rightarrow 4 \rightarrow 1$ constitute a SRH loop shown in Fig. 1(c).

Many theoretical studies on shock wave reflection have been done since SRH was first put forward [13], including investigations to determine the Mach stem height h_{m0} for stable MRs [21–27] and investigations on the stability of various reflection configurations [23,28–30]. Among these investigations, Li and Ben-Dor [29] applied the principle of minimum entropy production (MEP) to demonstrate that both RRs and MRs are stable in the dual-solution domain. This important basic work proved theoretically the possibility of SRH. MEP as a posteriori axiom [29] postulated by Glansdorff and Prigogine [31], has been found to predict the stability of a wide range of phenomena. Recent research [32] found that viscous dissipation, which is similar to entropy production but fulfills the mathematical conditions more strictly, should be considered as a Lagrangian in systems dominated by shock waves. In this paper we attempt to explain the mechanism behind this complex phenomenon using the minimal viscous dissipation (MVD) theorem.

The rest of this paper is organized as follows. In Sec. II, we present detailed information to calculate the total dissipation to apply MVD, with which the steady shock wave reflection can be determined. Particularly, in Sec. II A, we provide the proof of that a compressible flow should maintain MVD if three conditions are satisfied. In Sec. II B, we demonstrate that shock waves satisfy these three conditions and then should maintain MVD. In Sec. II C, we introduce flow structures in

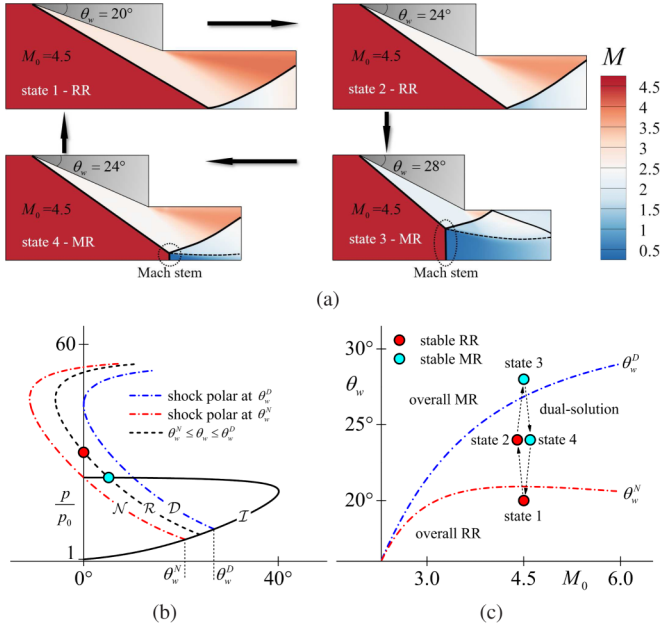*tangzhigong@126.com
†yangyanguang@cardc.cn

FIG. 1. (a) Hysteresis configurations of shock wave reflections for $M_0 = 4.5$ with colors representing the local Mach numbers M obtained by numerical computations, and simulation details are shown in Appendix A; (b) characteristic $(\theta, p/p_0)$-polars, where polars $\mathcal{I}$-$\mathcal{N}$ and $\mathcal{I}$-$\mathcal{D}$ correspond to θ_w^N and θ_w^D, respectively, and polar $\mathcal{I}$-$\mathcal{R}$ corresponds to the θ_w in the dual-solution domain; (c) variations of θ_w^D and θ_w^N with M_0 and the hysteresis loop induced by θ_w variation for $M_0 = 4.5$.

a shock reflection configuration and we analyze the order of magnitude of dissipation induced by different structures, indicating that a stable reflection configuration should maintain MVD. In Sec. II D, we compute the total dissipation of the reflection configuration depending on the Mach stem height and the wedge angle for a given inflow Mach number. In Sec. III, we display the total dissipation landscape, with whose geometric properties we explain the mechanism of shock reflection hysteresis. In addition, we also validate the present theory with previous experimental and numerical results. Finally, in Sec. IV, we conclude with a summary and a few open viewpoints. Some details of the derivation are relegated to the Appendices.

II. METHODS

In this section, we first introduce the definition of MVD and its scope of application in compressible flows. Then we explain the reason why a stable shock reflection configuration satisfies MVD. Finally we derive the relations of the total dissipation with the Mach stem height and wedge angle for a given inflow Mach number, with which we can obtain the total dissipation landscape shown in the next section.

A. MVD for compressible flows

Helmholtz and Rayleigh [33–35] proved that, for an incompressible viscous fluid, if the acceleration $\mathbf{a} = \mathbf{u} \cdot \nabla \mathbf{u}$ can be derived by a potential Γ, i.e., $\mathbf{a} = \nabla \Gamma$ or $\nabla \times \mathbf{a} = 0$, it should possess MVD, which is the well-known Helmholtz-

Rayleigh MVD theorem. Ho *et al.* [36,37] have tried to generalized this theorem to steady compressible flows, which satisfy

$$\nabla \cdot (\rho \mathbf{u}) = 0, \tag{1}$$

$$\rho \mathbf{u} \cdot \nabla \mathbf{u} = \rho \mathbf{f} - \nabla p + \nabla(\eta \Theta) + \nabla \cdot (2\mu \mathbf{D}), \tag{2}$$

$$\rho \mathbf{u} \cdot \nabla \left(\tfrac{1}{2} |\mathbf{u}|^2 \right) = \rho \mathbf{f} \cdot \mathbf{u} + p\Theta + \nabla \cdot (\mathbf{T} \cdot \mathbf{u}) - \phi, \tag{3}$$

where Eqs. (1)–(3) are the mass, momentum, and kinetic energy equations, respectively; ρ, $\mathbf{u}$, $\mathbf{f}$, p, η, and μ are the density, velocity, body force, pressure, dilatation viscosity, and shear viscosity, respectively. $\Theta = \nabla \cdot \mathbf{u}$, $\mathbf{D} = [\nabla \mathbf{u} + (\nabla \mathbf{u})^T]/2$ and $\mathbf{T} = (-p + \eta \Theta)\mathbf{I} + 2\mu \mathbf{D}$ are the velocity divergence, strain-rate tensor and stress tensor, respectively. ϕ is the viscous dissipation per unit volume:

$$\phi = \eta \Theta^2 + 2\mu \mathbf{D} : \mathbf{D}. \tag{4}$$

Here, we provide the proof process of MVD and clarify its applicable scope for compressible flows. The proof of MVD is mathematically a variational problem. The total dissipation Φ in a control volume V bounded by ℓ is considered, where V is nondeformable or the flow on ℓ (if V is deformable) is nondissipative. With the constraint provided by Eq. (1), the variation of Φ can be written as

$$\delta \Phi = \delta \int_V [\phi + \lambda \nabla \cdot (\rho \mathbf{u})] dV = 0, \tag{5}$$

where λ is a Lagrangian multiplier and $\mathcal{L} = \phi + \lambda \nabla \cdot (\rho \mathbf{u})$ is the Lagrangian. Because $\mathbf{u}$ and ρ are the two independent variables of $\mathcal{L}$, the Eular-Lagrangian equations are

$$\frac{\delta \mathcal{L}}{\delta \mathbf{u}} = 0 \Rightarrow \frac{\partial \mathcal{L}}{\partial \mathbf{u}} - \nabla \cdot \frac{\partial \mathcal{L}}{\partial \nabla \mathbf{u}} - \nabla \frac{\partial \mathcal{L}}{\partial \nabla \cdot \mathbf{u}} = 0, \tag{6}$$

$$\frac{\delta \mathcal{L}}{\delta \rho} = 0 \Rightarrow \frac{\partial \mathcal{L}}{\partial \rho} - \nabla \cdot \frac{\partial \mathcal{L}}{\partial \nabla \rho} = 0. \tag{7}$$

Substituting Eq. (4) into $\mathcal{L}$ and Eq. (6), we can obtain

$$\lambda \nabla \rho - \nabla \cdot [2\mu(\nabla \mathbf{u} + \nabla \mathbf{u}^T)] - \nabla[2\eta(\nabla \cdot \mathbf{u}) + \lambda \rho] = 0. \tag{8}$$

From Eq. (8), we can finally obtain

$$2[\nabla \cdot (2\mu \mathbf{D}) + \nabla(\eta \Theta)] + \rho \nabla \lambda = 0. \tag{9}$$

Substituting Eq. (4) into $\mathcal{L}$ and Eq. (7), we can obtain

$$\lambda \nabla \cdot \mathbf{u} - \nabla \cdot (\lambda \mathbf{u}) = 0. \tag{10}$$

From Eq. (10), we can finally obtain

$$\mathbf{u} \cdot \nabla \lambda = 0. \tag{11}$$

If a flow satisfies (i) $\mathbf{a} = \nabla \Gamma$; (ii) $\mathbf{f} = -\nabla U$, i.e., the body force can be derived by a potential U; (iii)$\nabla p/\rho = \nabla \int dp/\rho$ or $\nabla p \times \nabla \rho = 0$, i.e., the flow is barotropic, then the viscous force can be derived by a potential Π in Eq. (2), i.e., $[\nabla(\eta \vartheta) + \nabla \cdot (2\mu D)]/\rho = \nabla \Pi$. Thus, with λ chosen as $\lambda = -(\Gamma + \int dp/\rho + U + \Pi)$, Eqs. (9) and (11) can be exactly rearranged to Eqs. (2) and (3), respectively. Therefore, compressible flows satisfying (i), (ii), and (iii) must have minimal dissipation [32].

we have

$$\nabla \rho(x, y, z) \times \nabla p(x, y, z) = \mathcal{X}\mathbf{i} + \mathcal{Y}\mathbf{j} + \mathcal{Z}\mathbf{k} = \mathbf{0}, \quad (18)$$

where

$$\mathcal{X} = \left(\frac{\partial \rho}{\partial y}\frac{\partial p}{\partial z} - \frac{\partial \rho}{\partial z}\frac{\partial p}{\partial y}\right) = \begin{vmatrix} \frac{\partial \rho}{\partial y} & \frac{\partial \rho}{\partial z} \\ \frac{\partial p}{\partial y} & \frac{\partial p}{\partial z} \end{vmatrix} = 0,$$

$$\mathcal{Y} = \left(\frac{\partial \rho}{\partial z}\frac{\partial p}{\partial x} - \frac{\partial \rho}{\partial x}\frac{\partial p}{\partial z}\right) = -\begin{vmatrix} \frac{\partial \rho}{\partial x} & \frac{\partial \rho}{\partial z} \\ \frac{\partial p}{\partial x} & \frac{\partial p}{\partial z} \end{vmatrix} = 0, \quad (19)$$

$$\mathcal{Z} = \left(\frac{\partial \rho}{\partial x}\frac{\partial p}{\partial y} - \frac{\partial \rho}{\partial y}\frac{\partial p}{\partial x}\right) = \begin{vmatrix} \frac{\partial \rho}{\partial x} & \frac{\partial \rho}{\partial y} \\ \frac{\partial p}{\partial x} & \frac{\partial p}{\partial y} \end{vmatrix} = 0.$$

The flow is assumed nonuniform, i.e., there is some variation of ρ at least one direction (x, y, and z directions are all possible and equivalent). Here y direction is chosen, e.g., $\partial \rho/\partial y \neq 0$. Based on the implicit function theorem, the Jacobian is zero in Eq. (19), indicating that p can be written as an explicit function of ρ and x, without independent variables y and z, i.e.,

$$p = F[\rho(x, y, z), x] = F(\rho, x). \quad (20)$$

Substituting Eq. (20) into Eq. (19) (z direction), we have

$$\frac{\partial \rho}{\partial x}\frac{\partial p}{\partial y} - \frac{\partial \rho}{\partial y}\frac{\partial p}{\partial x}$$
$$= \frac{\partial \rho}{\partial x}\frac{\partial F(\rho, x)}{\partial \rho}\frac{\partial \rho}{\partial y} - \frac{\partial \rho}{\partial y}\left[\frac{\partial F(\rho, x)}{\partial \rho}\frac{\partial \rho}{\partial x} + \frac{\partial F(\rho, x)}{\partial x}\right]$$
$$= 0. \quad (21)$$

Simplifying Eq. (21), we have

$$\frac{\partial \rho}{\partial y}\frac{\partial F(\rho, x)}{\partial x} = 0. \quad (22)$$

Because $\partial \rho/\partial y \neq 0$, there must be

$$\frac{\partial F(\rho, x)}{\partial x} = 0. \quad (23)$$

Equation (23) means that $F(\rho, x)$ is independent of x, i.e.,

$$p = F(\rho, x) = F(\rho). \quad (24)$$

As the "y direction" in this proof is not specify in advance, once the density is not uniform, the condition $\partial \rho/\partial y \neq 0$ can be fulfilled with proper selection of "y direction." And if the density is constant, $p = F(\rho)$ is always true. Then the proof is completed, i.e., barotropic flow $p = F(\rho)$ can be confirmed with $\nabla \rho \times \nabla p = \mathbf{0}$.

Because conditions (i), (ii), and (iii) are all satisfied, a steady flow across an oblique straight shock wave should maintain MVD. Additionally, for a curved shock wave, if its curvature radius is much larger than its thickness, then every local segment of this curved shock can be regarded as a straight one, and this curved shock also maintains MVD.

C. MVD for shock reflection configurations

1. Flow structures in shock reflection configurations

Figure 3(a) shows the characteristic flow structures of an MR, including the shock waves, the expansion fan *RBC*, the
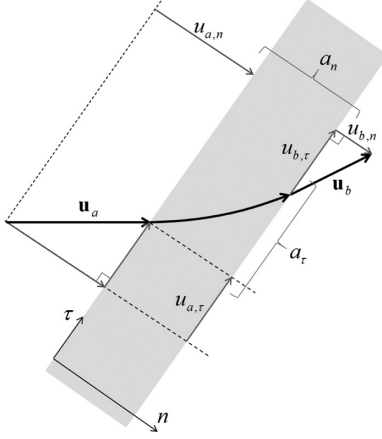

FIG. 2. A streamline across the shock wave.

B. MVD for shock waves

As shown in Fig. 2, a flow passing through an oblique straight shock wave (the gray region) is illustrated with a characteristic streamline, where $\mathbf{u}_a$ and $\mathbf{u}_b$ are the velocities ahead of and behind the shock wave. Let n and τ be the vertical and tangential directions relative to the shock front, respectively, then we have

$$\partial\mathbf{u}/\partial\tau = 0 \quad \text{and} \quad \partial\mathbf{a}/\partial\tau = 0. \quad (12)$$

Denote the vertical and tangential components of the acceleration $\mathbf{a}$ as a_n and a_τ, respectively, then Eq. (12) gives

$$\partial a_n/\partial\tau = \partial a_\tau/\partial\tau = 0. \quad (13)$$

Because the tangential components of $\mathbf{u}_a$ and $\mathbf{u}_b$ relative to the shock are equal, i.e., $u_{a,\tau} = u_{b,\tau}$, the tangential component a_τ of acceleration $\mathbf{a}$ must be zero, i.e., $a_\tau = 0$. Thus, we can obtain

$$\partial a_\tau/\partial n = 0. \quad (14)$$

Combine Eqs. (13) and (14) to obtain

$$|\nabla \times \mathbf{a}| = \partial a_\tau/\partial n - \partial a_n/\partial\tau = 0, \quad (15)$$

which means condition (i) is satisfied. Because the body force $\mathbf{f}$ is gravity and can be negligible, i.e., $\mathbf{f} \simeq 0$, condition (ii) can be satisfied as well.

For the density ρ and the pressure p, there also be $\partial\rho/\partial\tau = 0$ and $\partial p/\partial\tau = 0$. Let $\vec{e_\tau}$ and $\vec{e_n}$ be the unit vectors of directions τ and n, then $\nabla\rho$ and ∇p are given by

$$\nabla\rho = \frac{\partial\rho}{\partial\tau}\vec{e_\tau} + \frac{\partial\rho}{\partial n}\vec{e_n} = \frac{\partial\rho}{\partial n}\vec{e_n},$$

$$\nabla p = \frac{\partial p}{\partial\tau}\vec{e_\tau} + \frac{\partial p}{\partial n}\vec{e_n} = \frac{\partial p}{\partial n}\vec{e_n}. \quad (16)$$

Combining the two formulas in Eq. (16) can give

$$\nabla\rho \times \nabla p = \frac{\partial\rho}{\partial n}\vec{e_n} \times \frac{\partial p}{\partial n}\vec{e_n} = \mathbf{0}. \quad (17)$$

With Eq. (17), condition (iii) is satisfied. The detailed proof is shown as follows. Let x, y, and z be the spatial coordinates, corresponding the unit vectors $\mathbf{i}$, $\mathbf{j}$, and $\mathbf{k}$, respectively. Then
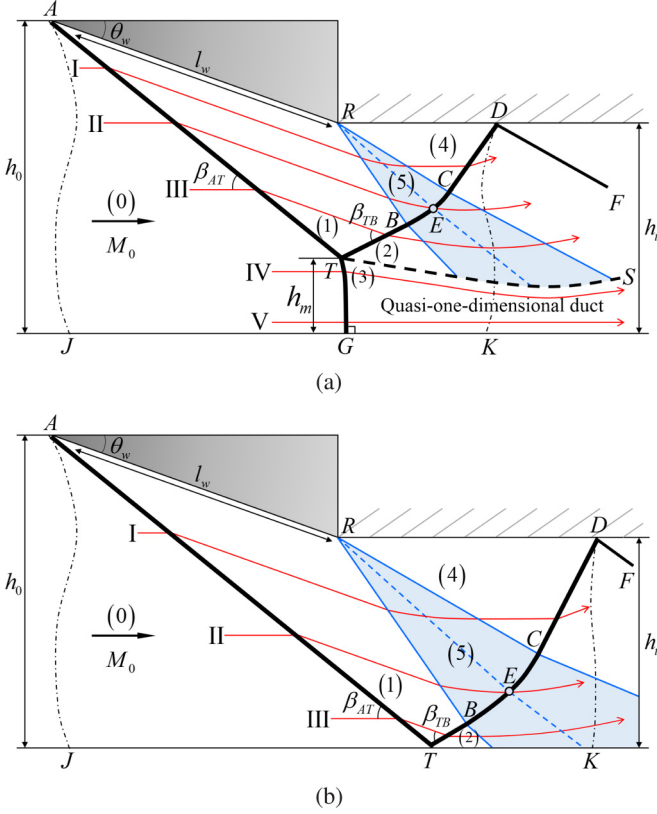
FIG. 3. Schematic diagrams of (a) an MR and (b) an RR.

quasi-one-dimensional duct flow, and the shear layer TS. The shock waves are composed of an incident shock wave AT, a Mach stem TG with a height of h_m, and a reflected shock wave including a straight segment TB, a curved segment BC and another straight segment CD. Five characteristic flow streamlines I–V are illustrated to show the flow features. Streamlines I–V are parallel in region (0), where I–III pass through shock AT and streamlines IV and V pass through TG. Behind shock AT, streamline I first experiences the isentropic expansion process and then enters into region (4), finally passing through shock CD; streamline II passes through shock BC at point E, which is inside the expansion fan; streamline III first passes through shock TB and then encounters the expansion fan. Behind shock TG, streamline IV first deflects slightly toward the reflecting surface JK at a subsonic speed, paralleling streamline III in region (2), and then gradually expands; streamline V continuously parallels the reflecting surface JK. Figure 3(b) shows the flow structures of an RR. Different from the MR, shock TG, the shear layer TS, and streamlines IV and V vanish and streamline III in region (2) parallels JK. A control volume V is chosen to enclose the reflection configuration. It is bounded by the upper wall ARD, the reflecting surface JK, the inflow surface AJ, and the outflow surface DK.

Figures 3(a) and 3(b) are in fact half-plane symmetrical RR and MR configurations with two symmetrical wedges analogous to those in experiments [9,15], respectively. In this case, the reflecting surface JK is the virtual symmetrical line rather than a nonslip solid wall, thus completely eliminating the development of a boundary layer along it.

2. Dissipation of different flow structures

For two-dimensional flows, Eq. (4) can be written in detail as

$$
\phi = \eta \left[\left(\frac{\partial u_\tau}{\partial \tau} \right)^2 + \left(\frac{\partial u_n}{\partial n} \right)^2 + 2 \left(\frac{\partial u_\tau}{\partial \tau} \frac{\partial u_n}{\partial n} \right) \right]
$$
$$
+ 2\mu \left[\left(\frac{\partial u_\tau}{\partial \tau} \right)^2 + \left(\frac{\partial u_n}{\partial n} \right)^2 + \left(\frac{\partial u_\tau}{\partial n} \right)^2 + \left(\frac{\partial u_n}{\partial \tau} \right)^2 \right],
$$

(25)

where n and τ are the orthogonal coordinates, and u_n and u_τ are the velocity components in n and τ directions, respectively. We will use Eq. (25) to analyze the magnitude order of the dissipation induced by different flow structures.

For a shock wave with length L_ω and characteristic thickness ϵ_ω, as shown in Fig. 4(a), we have $\partial u_\tau / \partial \tau \approx 0$, $\partial u_\tau / \partial n \approx 0$ and $\partial u_n / \partial \tau \approx 0$. Using Eq. (25), the dissipation ϕ_ω induced by this shock wave can be written as

$$
\phi_\omega = (\eta + 2\mu) \left(\frac{\partial u_n}{\partial n} \right)^2 \approx (\eta_\omega + 2\mu_\omega) \left(\frac{\Delta u_{\omega,n}}{\varepsilon_\omega} \right)^2, \quad (26)
$$

where $\Delta u_{\omega,n} = u_{a,n} - u_{b,n}$ is the characteristic velocity difference of this shock wave. η_ω and μ_ω are the characteristic dilatation viscosity and shear viscosity, respectively, defined as the values at the center line of this shock wave. Then the total dissipation Φ_ω can be approximate to

$$
\Phi_\omega \approx L_\omega \varepsilon_\omega (\eta_\omega + 2\mu_\omega) \left(\frac{\Delta u_{\omega,n}}{\varepsilon_\omega} \right)^2
$$
$$
= (\eta_\omega + 2\mu_\omega)(\Delta u_{\omega,n})^2 \frac{L_\omega}{\varepsilon_\omega}. \quad (27)
$$

For a shear layer with length L_s and characteristic thickness ϵ_s, as shown in Fig. 4(b), we have $\partial u_\tau / \partial \tau \approx 0$, $\partial u_\tau / \partial n \approx 0$ and $\partial u_n / \partial \tau \approx 0$. Using Eq. (25), the dissipation ϕ_s induced by this shear layer can be written as

$$
\phi_s = 2\mu \left(\frac{\partial u_\tau}{\partial n} \right)^2 \approx 2\mu_s \left(\frac{\Delta u_\tau}{\varepsilon_s} \right)^2. \quad (28)
$$

Where $\Delta u_{s,\tau} = u_{a,\tau} - u_{b,\tau}$ is characteristic velocity difference of this shear layer, and μ_s is the characteristic shear viscosity, defined as the value at the center line of this shear layer. Then the total dissipation Φ_s induced by this shear layer can be approximate to

$$
\Phi_s \approx L_s \varepsilon_s (2\mu_s) \left(\frac{\Delta u_{s,\tau}}{\varepsilon_s} \right)^2 = 2\mu_s (\Delta u_{s,\tau})^2 \frac{L_s}{\varepsilon_s}. \quad (29)
$$

For a quasi-one-dimensional duct flow with height L_d and characteristic thickness ϵ_d, as shown in Fig. 4(c), we have $u_n \approx 0$, $\partial u_\tau / \partial \tau \approx 0$, $\partial u_\tau / \partial n \approx 0$, and $\partial u_n / \partial \tau \approx 0$. Using Eq. (25), the dissipation ϕ_d induced by this quasi-one-dimensional duct flow can be written as

$$
\phi_d = (\eta + 2\mu) \left(\frac{\partial u_\tau}{\partial \tau} \right)^2 \approx (\eta_d + 2\mu_d) \left(\frac{\Delta u_{d,\tau}}{\varepsilon_d} \right)^2, \quad (30)
$$

where $\Delta u_{d,n} = u_{a,n} - u_{b,n}$ is the characteristic velocity difference of this quasi-one-dimensional duct flow. η_d and μ_d are the characteristic dilatation viscosity and shear viscosity of
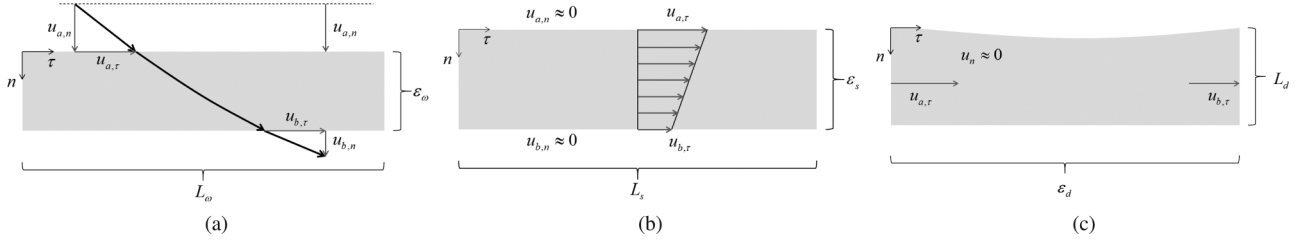
FIG. 4. Features of different flow structures. (a) A shock wave; (b) a shear layer; (c) a quasi-one-dimensional duct flow.

this duct flow, defined as the values at $\epsilon_d/2$. Then the total dissipation Φ_d induced by this shear layer can be approximate to

$$\Phi_d \approx L_d \varepsilon_d (\eta_d + 2\mu_d)\left(\frac{\Delta u_{d,\tau}}{\varepsilon_d}\right)^2$$
$$= (\eta_d + 2\mu_d)(\Delta u_{d,\tau})^2 \frac{L_d}{\varepsilon_d}. \qquad (31)$$

As a matter of fact, a quasi-one-dimensional duct flow can be regarded as an isentropic process and nondissipative.

In addition, a flow passing through an expansion fan is an isentropic process, so there is no viscosity dissipation in this process, i.e., the total dissipation induced by an expansion fan is zero.

Then we analyze the order of magnitude of dissipation induced by different flow structures. In the scale of global flow field, we have

$$L_\omega \sim L_s \sim L_d, \quad \Delta u_{\omega,n} \sim \Delta u_{s,\tau} \sim \Delta u_{d,\tau}$$
$$\eta_\omega + 2\mu_\omega \sim 2\mu_s \sim \eta_d + 2\mu_d, \quad \varepsilon_d \gg \varepsilon_s \gg \varepsilon_\omega. \qquad (32)$$

Substituting Eq. (32) into Eqs. (27), (29), and (31), we can obtain

$$\frac{\Phi_s}{\Phi_\omega} \sim \frac{\varepsilon_\omega}{\varepsilon_s} \to o(1), \quad \frac{\Phi_d}{\Phi_\omega} \sim \frac{\varepsilon_\omega}{\varepsilon_d} \to o(1). \qquad (33)$$

Equation (33) shows that the dissipation induced by the shear layer and the quasi-one-dimensional duct flow can be negligible relative to that induced by the shock waves. Besides, the expansion fan and the quasi-one-dimensional flow are isentropic and nondissipative. Consequently, the total dissipation of a shock wave reflection system is mainly contributed by the shock waves.

As demonstrated above, a steady shock wave configuration should maintain MVD. Since viscous dissipation in V is mainly contributed by shock waves, a stable reflection configuration, either an RR or an MR, should maintain the MVD. Using the Mach stem height h_m to represent a shock wave reflection state, for a stable configuration with h_{m0}, we have

$$\frac{\partial \Phi}{\partial h_m}\bigg|_{h_{m0}} = 0, \quad \frac{\partial^2 \Phi}{\partial h_m^2}\bigg|_{h_{m0}} > 0. \qquad (34)$$

D. The total dissipation of a shock reflection configuration

Here we compute the total dissipation Φ in a shock reflection configuration and provide its dependence on the Mach stem height h_m and wedge angle θ_w for a given Mach number

M_0. Without loss of generality, Φ in V can be written as

$$\Phi = \sum_i \Phi_i = \sum_i \int \phi_i d\sigma_i, \qquad (35)$$

where ϕ and σ are the dissipation induced per unit length of shock i and the length of this shock, respectively. These quantities are closely related to the flow properties and geometric relations. The flow properties on both sides of shock wave i ($i = AT, TG, TB, BC, CD$) satisfy

$$M_{b,i} = \mathcal{F}_M(M_{a,i}, \beta_i), \quad p_{b,i}/p_{a,i} = \mathcal{F}_p(M_{a,i}, \beta_i),$$
$$\rho_{b,i}/\rho_{a,i} = \mathcal{F}_\rho(M_{a,i}, \beta_i), \quad \mathcal{A}_{b,i}/\mathcal{A}_{a,i} = \mathcal{F}_\mathcal{A}(M_{a,i}, \beta_i),$$
$$\mathcal{F}_\beta(M_{a,i}, \beta_i, \theta_i) = 0, \qquad (36)$$

where functions $\mathcal{F}_M$, $\mathcal{F}_p$, $\mathcal{F}_\rho$, $\mathcal{F}_\mathcal{A}$, and $\mathcal{F}_\beta$ are the classical Rankine-Hugoniot relations [38–40] and shown in part 1 of Appendix B. Subscripts "a" and "b" denote variables ahead of and behind the shock wave i, respectively. $\mathcal{A}$, θ, and β are the acoustic speed, the flow deflection angle and the shock angle (the angle between the incoming flow and the shock wave), respectively. Flow properties ahead of point E on shock BC inside the expansion fan satisfy

$$\mathcal{H}_{P-M}(M_{a,E}, M_{b,AT}, \alpha_{a,E}, \theta_w) = 0,$$
$$p_{a,E}/p_{b,AT} = \mathcal{H}_p(M_{a,E}, M_{b,AT}),$$
$$\rho_{a,E}/\rho_{b,AT} = \mathcal{H}_\rho(M_{a,E}, M_{b,AT}),$$
$$\mathcal{A}_{a,E}/\mathcal{A}_{b,AT} = \mathcal{H}_\mathcal{A}(M_{a,E}, M_{b,AT}), \qquad (37)$$

where $\mathcal{H}_{P-M}$, $\mathcal{H}_p$, $\mathcal{H}_\rho$, and $\mathcal{H}_\mathcal{A}$ are the Prandtl-Meyer expansion fan relations [41,42] and shown in part 2 of Appendix B, and $\alpha_{a,E}$ is the flow (ahead of point E) deflection angle relative to the reflecting surface JK. Additionally, let the coordinates of point A be $(x_A, y_A) = (0, 0)$, we have $(x_R, y_R) = (l_w \cos\theta_w, -l_w \sin\theta)$ and $(x_T, y_T) = [(h_0 - h_m)\cot\beta_{AT}, -(h_0 - h_m)]$, where h_0 and l_w are the inflow height and the wedge length, respectively. Thus, the coordinates of point B, E, C, and D satisfy

$$y_B - y_T = (x_B - x_T)\tan(\beta_{TB} - \theta_{AT}),$$
$$y_B - y_R = (x_B - x_R)\tan\left(\arctan\frac{1}{M_1} + \theta_{AT}\right),$$
$$\mathcal{G}_E(M_R, \alpha_{a,E}, \beta_E, x_E, y_E) = 0,$$
$$(x_E, y_E) = (x_B, y_B), \quad \text{when } \alpha_{a,E} = \theta_w,$$
$$(x_C, y_C) = (x_E, y_E), \quad \text{when } \alpha_{a,E} = 0,$$
$$y_D - y_C = (x_D - x_C)\tan\beta_{CD},$$
$$y_D = -l_w \sin\theta_w, \qquad (38)$$

where function $\mathcal{G}_E$ is the differential relations depicting the interactions of the expansion fan and shock BC derived by Bai *et al.* [25]. Note that shock TB is the initial segment of the reflected shock wave, which plays a crucial role in determining the shape and strength of the other two segments BC and CD; hence, shock angle β_{TB} and the Mach stem height h_m are two pivotal parameters of the shock wave reflection system. For stable configurations, $\beta_{TB}(RR)$ of a stable RR with $h_m = 0$ and $\beta_{TB}(MR)$ of a stable MR with $h_m = h_{m0}$ can be obtained by the two- and three-shock theories [11,12], respectively, see also Appendix C for more details. Additionally, for a given combination of M_0 and θ_w, there is always $\beta_{TB}(RR) > \beta_{TB}(MR)$. For an unstable reflection (UR) in an RR $\rightleftharpoons$ MR transition, Mouton & Hornung [23] assumed that the configuration contains only a single but evolutionary MR. Gao and Wu [30] found that an UR has more detailed structures at the beginning of the RR $\rightleftharpoons$ MR transition; these are induced by an upstream disturbance. In this paper, we consider URs as possible unsteady states just maintain unsteady MR configurations with Mach stem heights h_m. As h_m increases monotonically from 0 to h_{m0}, the shock angle β_{TB} should decrease monotonically from $\beta_{TB}(RR)$ to $\beta_{TB}(MR)$. The dimensionless forms of β_{TB} and h_m are written as $\beta_{TB}^* = [\beta_{TB} - \beta_{TB}(MR)]/[\beta_{TB}(RR) - \beta_{TB}(MR)]$ and $h_m^* = h_m/h_{m0}$, respectively, where $\beta_{TB}^* = 1$ when $h_m^* = 0$ and $\beta_{TB}^* = 0$ when $h_m^* = 1$. In consideration of physical reality that the shear layer TS should not touch the reflecting surface JK [23] when a stable RR just changes into an UR, we propose that $(d\beta_{TB}^*/dh_m^*)_{h_m^*=0} = 0$. When the UR approaches becoming a stable MR, i.e., $h_m^* \rightarrow 1$, β_{TB}^* is assumed to vary linearly. Therefore, to satisfy the above conditions, β_{TB}^* can be approximated to

$$\beta_{TB}^* = \mathcal{W}_{\beta_{TB}^*}(h_m^*) \simeq \cos\left(h_m^* \cdot \frac{\pi}{2}\right), \quad (39)$$

where $\mathcal{W}_{\beta_{TB}^*}$ is an approximate function that constructs the relation between β_{TB}^* and h_m^*. Based on Eq. (38), we can obtain the coordinates of points $T(x_T, y_T)$, $B(x_B, y_B)$, $C(x_C, y_C)$, $D(x_D, y_D)$, and $E(x_T, y_T)$, then the length of the straight shock waves AT, TB, and CD can be written as

$$\begin{aligned} \sigma_{AT} &= \sqrt{x_T^2 + y_T^2}, \\ \sigma_{TB} &= \sqrt{(x_B - x_T)^2 + (y_B - y_T)^2}, \\ \sigma_{CD} &= \sqrt{(x_D - x_C)^2 + (y_D - y_C)^2}. \end{aligned} \quad (40)$$

For the dissipation ϕ_i induced by per unit length of a shock wave i, since viscous dissipation is the dominant term of kinetic energy loss in compressible flows [43,44], it can be approximated to

$$\phi_i \simeq \tfrac{1}{2}\rho_{a,i}(M_{a,i}\mathcal{A}_{a,i}\sin\beta_i)^3 - \tfrac{1}{2}\rho_{b,i}[M_{b,i}\mathcal{A}_{b,i}\sin(\beta_i - \theta_i)]^3. \quad (41)$$

Combine Eqs. (40) and (41), and we can obtain the total dissipation induced by the straight shock waves:

$$\begin{aligned} \Phi_{AT} &= \phi_{AT}\sigma_{AT}, \\ \Phi_{TB} &= \phi_{TB}\sigma_{TB}, \\ \Phi_{CD} &= \phi_{CD}\sigma_{CD}. \end{aligned} \quad (42)$$

For the Mach stem, since it is just slightly curved, its length σ_{TG} can be approximate to its height h_m, and the dissipation can be approximate to

$$\Phi_{TG} \simeq \tfrac{1}{2}(\phi_{T(3)} + \phi_G)h_m. \quad (43)$$

Where subscripts "$T(3)$" and "G" correspond to the parts of shock TG near the triple point T and the shock foot G, respectively. $\beta_{T(3)}$ has been obtained in part 2 of Appendix C, and $\beta_G = \pi/2$. Using the flow properties near points T and G, we can calculate $\phi_{T(3)}$, ϕ_G, and then the total dissipation Φ_{TG} induced by shock TG.

For the curved shock BC, the infinitesimal length near point E can be written as

$$d\sigma_E = \sqrt{(dx_E)^2 + (dy_E)^2}. \quad (44)$$

Thus, the dissipation induced by BC can be written as

$$\Phi_{BC} = \int_B^C \phi_E d\sigma_E. \quad (45)$$

As the flow properties near point E can be obtained with Ref. [25], we can calculate ϕ_E using Eq. (41). Then we can obtain the total dissipation Φ_{BC} induced by shock BC.

Combining Eqs. (40)–(45), we can obtain the total dissipation induced by the shock waves:

$$\Phi(\theta_w, h_m) = \Phi_{AT} + \Phi_{TB} + \Phi_{BC} + \Phi_{CD} + \Phi_{TG}. \quad (46)$$

As a result, for a given Mach number M_0, we can obtain the dependence of the total dissipation Φ on both the wedge angle θ_w and the Mach stem height h_m.

III. RESULTS AND DISCUSSIONS

In this section, we expound the mechanism of shock reflection hysteresis using the MVD theorem. The combination of Eqs. (34)–(46) gives the total dissipation $\Phi(\theta_w, h_m/h_0)$, depending on $\theta_w \in [\theta_w^N, \theta_w^D]$ and h_m/h_0. For $M_0 = 4.5$ with dual-solution domain $\theta_w \in [\theta_w^N, \theta_w^D] = [20.92°, 26.85°]$, the landscape of $\Phi(\theta_w, h_m/h_0)$ is illustrated in Fig. 5(b). Five characteristic wedge angles, $\theta_w = 21°, 22.5°, 24°, 25.5°$, and $26.5°$, are chosen to depict the dissipation features of the shock reflection configuration. As shown in Fig. 5(a), the initial state is set as a stable RR with $\theta_w = 21°$, at which angle the possible MR is highly unstable. This means that just a small disturbance would transform the MR (if it exists) to an RR. As θ_w increases to $22.5°$, a dissipation barrier emerges and two minimal dissipation values will be formed, corresponding to one stable RR at $\Phi(22.5°, 0)$ and one MR at $\Phi(22.5°, h_{m0}/h_0)$. If θ_w varies continuously and slowly, the disturbance will not be strong enough to transform the RR into an MR; then the configuration maintains a stable RR. The situation is similar as θ_w increases to $24°$; the only difference is that $\Phi(24°, 0) > \Phi(24°, h_{m0}/h_0)$, but $\Phi(22.5°, 0) < \Phi(22.5°, h_{m0}/h_0)$, meaning that the MR becomes more stable. When θ_w increases to $25.5°$, the RR becomes unstable and just a small disturbance can transform it into an MR. Once $\theta_w > 25.5°$, the configuration will maintain a stable MR.

As shown in Figs. 5(b) and 5(c), the transition point $\theta_w = 25.5°$ is a saddle-node bifurcation on the Φ landscape, i.e., the intersection point of the valley line $\Phi(\theta_w \leqslant 25.5°, 0)$ and
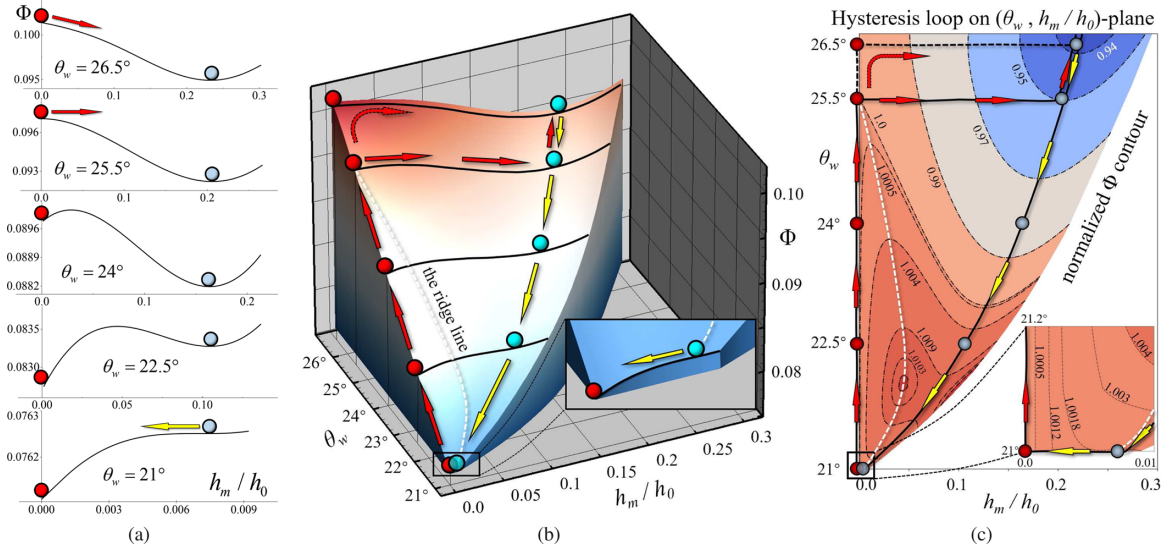
FIG. 5. Different perspectives of the total dissipation Φ landscape, where red (with $h_m/h_0 = 0$ on the left side of each subfigure) and blue (with $h_m/h_0 > 0$) spheres correspond to stable RRs and MRs, respectively. (a) Five latitude lines from the front view of the Φ landscape, with Φ versus h_m/h_0 at $\theta_w = 21°$, $22.5°$, $24°$, $25.5°$, and $26.5°$; (b) the Φ landscape, where red (pointing up or right) and yellow (pointing down or left) arrows show the paths of RR $\rightarrow$ MR and RR $\leftarrow$ MR in the valley, respectively, and the white dashed line is the ridge line; (c) contour of normalized total dissipation $\Phi/\Phi(\theta_w, 0)$, where the black solid line denotes the hysteresis loop of the RR $\rightleftharpoons$ MR transition and the black dashed line denotes the path when $\theta_w > 25.5°$.

the ridge line. Although stable RRs are possible theoretically when $\theta_w < 25.5°$, if θ_w decreases again from $26.5°$, then the configuration will remain as stable MRs until θ_w reaches $21°$. Thereafter, a small disturbance will transform the MR into an RR. The transition point $\theta_w = 21°$ is another saddle-node bifurcation, i.e., the intersection point of the valley line $\Phi(\theta_w \leqslant 26.5°, h_m/h_0 = h_{m0}/h_0)$ and the ridge line. As θ_w varies from $21°$ to $26.5°$ and then back to $21°$, a 3D path in the valleys of the $\Phi(\theta_w, h_m/h_0)$ landscape emerges, manifesting a series of stable configurations. Clearly, the projection of the path onto the $(\theta_w, h_m/h_0)$ plane is the hysteresis loop, as shown in Fig. 5(c). In addition, it is seen that the MR $\rightarrow$ RR transition occurs very close to $\theta_w^N = 20.92°$, while the RR $\rightarrow$ MR transition takes place at about $25.5°$; this angle is smaller than $\theta_w^D = 26.85°$. The transition point of RR $\rightarrow$ MR is less than θ_w^D, which was also observed by Chpoun *et al.* [15]. This is for the reason that MRs have larger stable regions than those of RRs in the dual-solution domain.

Furthermore, as cross validation, we compare the h_{m0} obtained by the present theory with previous experimental, numerical, and theoretical results at $M_0 = 3.98$, as shown in Fig. 6. The various data have been extracted directly from the quoted papers, then some inaccuracies may likely have occurred and should be treated with caution. For relatively small $\beta_{AT} < 35°$, the present theory compares remarkably well with experimental [45,46] and numerical [18] results. For relatively large $\beta_{AT} > 36°$, the theoretical results match very well with experimental [46] and numerical [18,23] results. When $35° < \beta_{AT} < 36°$, theoretical results reach values slightly larger than for experimental [46] and numerical [23] results. In general, the present theory is reasonable and valid.

Here, the cosine Eq. (39) is only an approximate function and is not universal for all inflow Mach numbers. Moreover,

the analytic expression of $\mathcal{W}_{\beta_{TB}^*}$ may be complicated and requires more in-depth research. More accurate models with more detailed structures describing the evolution of URs will be considered in the future.
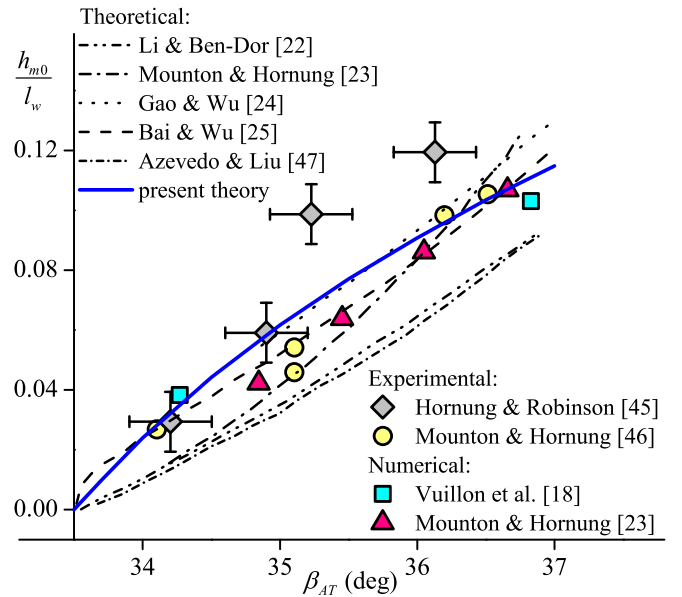

FIG. 6. Comparison of results using the present theory with those from previous works at $M_0 = 3.98$ and $|h_0 - y_R|/l_w \approx 0.4$, including experimental results from Hornung *et al.* [45,46], numerical results from Mouton and Hornung [23] and Vuillon *et al.* [18], and theoretical results from Azevedo and Liu [47], Li and Ben-Dor [22], Mouton and Hornung [23], Gao and Wu [24], and Bai and Wu [25].

IV. CONCLUSIONS

In this paper, the mechanism of hysteresis in shock wave reflection is studied. The steady states of shock wave reflection systems should maintain MVD. Therefore, a hysteresis loop is the projection of dissipation landscape valley lines onto the $(\theta_w, h_m/h_0)$ plane. The saddle-node bifurcations, i.e., intersection points of valley and ridge lines, are actually transition points. Therefore, the emergence and disappearance of the dissipation barriers, manifested by the ridge line of the dissipation landscape, are the origin of the reflection hysteresis.

The present method, based on the least-action principle and the geometric properties of the action surface, may be extended and applied to other hysteretic systems such as ferromagnetic systems [1], liquid-solid phase transitions [48,49], laminar-turbulent flow transitions [50–53], and Bose-Einstein condensations [54–57].

APPENDIX A: COMPUTATIONAL SETUP

1. Governing equations

The governing equations are the nondimensionalized conservative forms of the continuity, momentum and energy equations in curvilinear coordinates. In vector notation, these equations can be expressed as

$$\frac{\partial U}{\partial t} + \frac{\partial F}{\partial \xi} + \frac{\partial G}{\partial \zeta} = 0, \tag{A1}$$

where $U = J\{\rho, \rho u, \rho v, \rho e\}$ denotes the conservative vector flux, with ρ the density, e the energy per volume, and (u, v) velocity components of streamwise and vertical directions, respectively. J is the Jacobian matrix transforming Cartesian coordinates (x, y) into computational coordinates (ξ, ζ). F is the flux term in ξ direction as

$$
\begin{aligned}
F &= F_c + F_v \\
&= Jr_\xi \begin{bmatrix} \rho u^* \\ \rho u u^* + p s_x \\ \rho v u^* + p s_y \\ (\rho e + p) u^* \end{bmatrix} - Jr_\xi \begin{bmatrix} 0 \\ s_x \sigma_{xx} + s_y \sigma_{xy} \\ s_x \sigma_{yx} + s_y \sigma_{yy} \\ s_x \tau_x + s_y \tau_y \end{bmatrix}, \tag{A2}
\end{aligned}
$$

where

$$u^* = u s_x + v s_y, \quad s_x = \xi_x/r_\xi, \quad s_y = \xi_y/r_\xi, \quad r_\xi = \sqrt{\xi_x^2 + \xi_y^2},$$

$$\tau_x = u\sigma_{xx} + v\sigma_{yx} - q_x, \quad \tau_y = u\sigma_{xy} + v\sigma_{yy} - q_y,$$

$$\sigma_{ij} = 2\mu \left[\frac{1}{2}\left(\frac{\partial u_i}{\partial x_j} + \frac{\partial u_j}{\partial x_i} \right) - \frac{1}{3}\frac{\partial u_k}{\partial x_k}\delta_{ij} \right],$$

$$q_j = -\frac{\mu}{\text{Pr}(\gamma - 1)M_0^2}\frac{\partial T}{\partial x_j}. \tag{A3}$$

In above equations, F_c and F_v are the convective and the viscous terms, respectively. The flux term G in ζ direction has similar forms as F. p and T are the pressure and temperature,
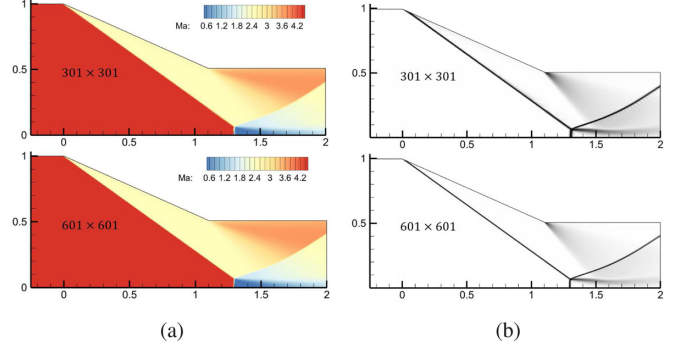

FIG. 7. Validation of grid convergence with two mesh scales. Upper: 301×301; lower: 601×601. (a) Flow fields colored by local Mach number; (b) numerical schlierens.

respectively. The work fluid is considered as ideal gas, i.e., $p = \rho T/\gamma M_0^2$ with the ratio of specific heats $\gamma = 1.4$ and inflow Mach number $M_0 = 4.5$, where subscript "0" represents the free-stream conditions. The characteristic Reynolds number $\text{Re} = 3000$ based on the inflow height, and Prandtl number $\text{Pr} = 0.7$. The viscosity μ fulfills the Sutherland law:

$$\mu = \frac{1}{\text{Re}} \frac{T^{3/2}(1 + T_s/T_0)}{T + T_s/T_0}, \tag{A4}$$

where $T_s = 110.4$ K and the free-stream temperature $T_0 = 108.1$ K.

2. Numerical methods

The present simulations are completing by the in-house code OPENCFD-SC. This code has been valided with a wide range of supersonic and hypersonic flow problems, such as SBLIs in a compression ramp, hypersonic boundary layer over a blunt cone and homogeneous isotropic turbulence [32,58–61]. For the flux term computation, the convective term is dealed with Steger-Warming splitting and solved by using WENO-SYMBO method, which is an optimized WENO scheme in a nine-point central stencil with a fourth order accuracy. With a limiter technique based on the total variation, the numerical dissipation and the computation cost is greatly reduced. The viscous flux terms are calculated with eighth-order central difference scheme. Three order TVD-type Runge-kutta method is used for time-advance [62].

3. Grid convergence study

The grid scales are chosen as 1201×601 for state 1-RR, 901×601 for state 2-RR, and 601×601 for both state 3-MR and state 4-MR. The normal grid spacing Δy is uniform at different streamwise location (for instance, $\Delta y_0 = h_0/600$ at the entrance); the streamwise grid is uniformly spacing with width $\Delta x_0/\Delta y_0 = 1.375$. As shown in Figs. 7(a) and 7(b), the grid convergence is validated with two grid scales,
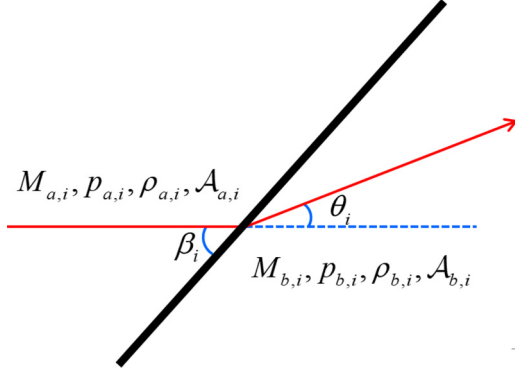
FIG. 8. Schematic diagram of a flow passing through a shock wave.

601 × 601 and 301 × 301, using state 4-MR colored by local Mach number. It can be seen in both Figs. 7(a) and 7(b) that locations of shock waves, triple points, shear layers, and Mach stems are the same between these two grid scales. For instance, locations of the feet of Mach stems are both at $x \approx 1.3$, indicating the grid scale 601 × 601 we used is suitable.

APPENDIX B: LAWS OF SHOCK WAVE, EXPANSION FAN, AND THEIR INTERACTIONS

1. The classical Rankine-Hugoniot relations

The classical Rankine-Hugoniot relations give the relations of the flow properties on both sides of shock wave i:

$$\mathcal{F}_M(M_{a,i}, \beta_i) = \frac{M_{a,i}^2 + \frac{2}{\gamma-1}}{\frac{2\gamma}{\gamma-1}M_{a,i}^2 \sin^2 \beta_i - 1} + \frac{M_{a,i}^2 \cos^2 \beta_i}{\frac{\gamma-1}{2}M_{a,i}^2 \sin^2 \beta_i + 1},$$

$$\mathcal{F}_p(M_{a,i}, \beta_i) = \frac{2\gamma}{\gamma+1}M_{a,i}^2 \sin^2 \beta_i - \frac{\gamma-1}{\gamma+1},$$

$$\mathcal{F}_\rho(M_{a,i}, \beta_i) = \frac{(\gamma+1)M_{a,i}^2 \sin^2 \beta_i}{(\gamma-1)M_{a,i}^2 \sin^2 \beta_i + 2} \tag{B1}$$

$$\mathcal{F}_\mathcal{A}(M_{a,i}, \beta_i) = \frac{\left[(\gamma-1)M_{a,i}^2 \sin^2 \beta_i + 2\right]^{1/2}\left[2\gamma M_{a,i}^2 \sin^2 \beta_i - (\gamma-1)\right]^{1/2}}{(\gamma+1)M_{a,i}\sin \beta_i},$$

$$\mathcal{F}_\beta(M_{a,i}, \beta_i, \theta_i) = 2\cot\beta \frac{M_{a,i}^2 \sin^2 \beta_i - 1}{M_{a,i}^2(\gamma + \cos 2\beta_i) + 2} - \tan \theta_i.$$

Where subscripts "a" and "b" denote variables ahead of and behind the shock wave i, respectively. $\gamma = 1.4$ is the specific heat ratio. M, p, ρ, and $\mathcal{A}$ are the flow Mach number, pressure, density, and acoustic speed, respectively. β is the shock angle (the angle between the incoming flow and the shock wave), and θ is the flow deflection angle across shock i. The flow passing through shock i is shown in Fig. 8.

2. The Prandtl-Meyer expansion relations

The Prandtl-Meyer expansion relations give the relations of the flow properties in an expansion fan:

$$\mathcal{H}_{\mathcal{P}-\mathcal{M}}(M_2, M_1, \alpha, \theta) = v(M_2) - v(M_1) - (\alpha - \theta) = 0,$$

$$\frac{p_2}{p_1} = \mathcal{H}_p(M_2, M_1) = \left[\frac{\vartheta(M_1)}{\vartheta(M_2)}\right]^{\frac{\gamma}{\gamma-1}},$$

$$\frac{\rho_2}{\rho_1} = \mathcal{H}_\rho(M_2, M_1) = \left[\frac{\vartheta(M_1)}{\vartheta(M_2)}\right]^{\frac{1}{\gamma-1}},$$

$$\frac{\mathcal{A}_2}{\mathcal{A}_1} = \mathcal{H}_\mathcal{A}(M_2, M_1) = \left[\frac{\vartheta(M_1)}{\vartheta(M_2)}\right]^{\frac{1}{2}},$$

$$v(M) = \sqrt{\frac{\gamma+1}{\gamma-1}} \arctan\sqrt{\frac{\gamma-1}{\gamma+1}(M^2-1)}$$
$$- \arctan\sqrt{M^2-1},$$

$$\vartheta(M) = 1 + \frac{\gamma-1}{2}M^2. \tag{B2}$$

The flow passing through the expansion fan is shown in Fig. 9.

APPENDIX C: THE SHOCK WAVE ANGLE OF A STABLE REFLECTION CONFIGURATION

1. The two-shock theory for a stable RR

The two-shock theory (2ST) is the analytical for describing the flow field of an RR near the reflection point T. Applying the Rankine-Hugoniot relations on the two oblique shock waves, AT and TB, as shown in Fig. 3(b), we can obtain the following equations.

Across the incident shock AT:

$$\mathcal{F}_\beta(M_0, \beta_{AT}, \theta_w) = 0,$$
$$M_{b,AT} = \mathcal{F}_M(M_0, \beta_{AT}), \tag{C1}$$
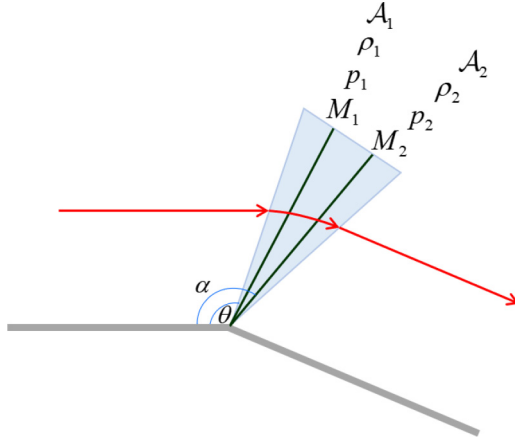
where subscript "0" denotes the inlet flow.

FIG. 9. Schematic diagram of a flow passing through an expansion fan.

Across the reflected shock TB:

$$\mathcal{F}_\beta(M_{b,AT}, \beta_{TB}, \theta_{TB}) = 0. \tag{C2}$$

Because the flow behind shock TB must be parallel to the reflecting surface JK in a stable RR, we have

$$\theta_{TB} - \theta_w = 0. \tag{C3}$$

The above set of four equations consists of only four parameters, namely: β_{AT}, $M_{b,AT}$, β_{TB}, and θ_w. We only consider AT and TB as weak shock waves, then the Eqs. (C1)–(C3) result in a unique solution, and we can obtain the shock wave β_{TB} for an RR, i.e., $\beta_{TB}(RR)$.

2. The three-shock theory for a stable MR

The three-shock theory (3ST) is the analytical for describing the flow field of a MR near the triple point T. Applying the Rankine-Hugoniot relations on the three shock waves AT, TB

and TG, as shown in Fig. 3(a), we can obtain the following equations.

Across the incident shock AT:

$$\mathcal{F}_\beta(M_0, \beta_{AT}, \theta_w) = 0,$$
$$M_{b,AT} = \mathcal{F}_M(M_0, \beta_{AT}),$$
$$\frac{p_{b,AT}}{p_0} = \mathcal{F}_p(M_0, \beta_{AT}). \tag{C4}$$

Across the reflected shock TB:

$$\mathcal{F}_\beta(M_{b,AT}, \beta_{TB}, \theta_{TB}) = 0,$$
$$\frac{p_{b,TB}}{p_{b,AT}} = \mathcal{F}_p(M_{b,AT}, \beta_{TB}). \tag{C5}$$

Across the Mach stem TG near point T:

$$\mathcal{F}_\beta(M_0, \beta_{T(3)}, \theta_{T(3)}) = 0,$$
$$\frac{p_{b,T(3)}}{p_0} = \mathcal{F}_p(M_0, \beta_{T(3)}), \tag{C6}$$

where subscripts $T(3)$ is the part of shock TG near the triple point T.

The flow states (2) and (3) are separated by a contact surface, across which the pressure remains constant, i.e.,

$$p_{b,T(3)} = p_{b,TB}. \tag{C7}$$

Additionally, the streamlines in regions (2) and (3) are parallel, i.e.,

$$\theta_w - \theta_{TB} = \theta_{T(3)}. \tag{C8}$$

The above set of nine equations consists of nine parameters, namely: β_{AT}, $M_{b,AT}$, $p_{b,AT}$, β_{TB}, θ_{TB}, $p_{b,TB}$, $\beta_{T(3)}$, $\theta_{T(3)}$, and $p_{b,T(3)}$. We consider AT and TB as weak shock waves and TG as a strong shock wave, then equations Eqs. (C4)–(C8) result in a unique solution, and we can obtain the shock wave β_{TB} for a MR, i.e., $\beta_{TB}(MR)$.

[1] M. Plischke and B. Bergersen, *Equilibrium Statistical Physics* (World Scientific, Singapore, 2006).

[2] I. Mayergoyz, *Mathematical Models of Hysteresis and Their Applications* (Elsevier, Amsterdam, 2003).

[3] A. Visintin, *Differential Models of Hysteresis*, Vol. 111 (Springer Science & Business Media, Berlin, 2013).

[4] F. Preisach, Z. Phys. **94**, 277 (1935).

[5] R. Bouc, in *Proceedings of the 4th Conference on Nonlinear Oscillations, Prague, Czechoslovakia* (1967).

[6] R. Bouc, Acustica **21**, 16 (1971).

[7] Y.-K. Wen, J. Eng. Mech. Div. **102**, 249 (1976).

[8] P. Jung, G. Gray, R. Roy, and P. Mandel, Phys. Rev. Lett. **65**, 1873 (1990).

[9] G. Ben-Dor and G. Ben-Dor, *Shock Wave Reflection Phenomena*, Vol. 2 (Springer, Berlin, 2007).

[10] E. Mach, Sitzungsbr. Akad. Wiss. Wien **78**, 819 (1878).

[11] J. von Neumann, Bureau of Ordinance, Explosives Research Report (1943).

[12] J. Von Neumann, NAVORD Rep. 203-45 (1945).

[13] H. G. Hornung, H. Oertel, and R. J. Sandeman, J. Fluid Mech. **90**, 541 (1979).

[14] A. Chpoun, D. Passerel, J.-C. Lengrand, H. Li, and G. Ben-Dor, C. R. Acad. Sci., Ser. II **319**, 1447 (1994).

[15] A. Chpoun, D. Passerel, H. Li, and G. Ben-Dor, J. Fluid Mech. **301**, 19 (1995).

[16] V. Fomin, H. Hornung, M. Ivanov, A. Kharitonov, G. Klemenkov, A. Kudryavtsev, and A. Pavlov, in *Proceedings of the 12th International Mach Reflection Symposium, Pilanesberg, South Africa* (1996), pp. 137–151.

[17] M. Ivanov, A. Kharitonov, G. Klemenkov, A. Kudryavtsev, and V. Fomin, in *Proceedings of the 13th International Mach Reflection Symposium, Israel, Vol. 3* (1998), p. 68.

[18] J. Vuillon, D. Zeitoun, and G. Ben-Dor, J. Fluid Mech. **301**, 37 (1995).

[19] A. Chpoun and G. Ben-Dor, Shock Waves **5**, 199 (1995).

[20] M. Ivanov, G. Ben-Dor, T. Elperin, A. Kudryavtsev, and D. Khotyanovsky, AIAA J. **39**, 972 (2001).

[21] D. Azevedo, Ph.D. thesis, State University of New York (1989).

[22] H. Li and G. Ben-Dor, J. Fluid Mech. **341**, 101 (1997).

[23] C. A. Mouton and H. G. Hornung, AIAA J. **45**, 1977 (2007).

[24] B. Gao and Z. Wu, J. Fluid Mech. **656**, 29 (2010).

[25] C.-Y. Bai and Z.-N. Wu, J. Fluid Mech. **818**, 116 (2017).

[26] S. Roy and R. Gopalapillai, J. Fluid Mech. **863**, 242 (2019).

[27] C. Wang, L. Xue, and K. Cheng, J. Fluid Mech. **857**, 784 (2018).

[28] V. M. Teshukov, J. Appl. Mech. Tech. Phys. **30**, 189 (1989).

[29] H. Li and G. Ben-Dor, J. Appl. Phys. **80**, 2027 (1996).

[30] S. Li, B. Gao, and Z. Wu, J. Fluid Mech. **682**, 160 (2011).

[31] P. Glansdorff and I. Prigogine, *Thermodynamic theory of structure, stability and fluctuations* (Wiley-Interscience, 1971).

[32] Y.-C. Hu, W.-F. Zhou, Y.-G. Yang, and Z.-G. Tang, Phys. Fluids **32**, 101702 (2020).

[33] H. v. Helmholtz, Wiss. Abh **1**, 223 (1868).

[34] L. Rayleigh, London, Edinburgh, Dublin Philos. Mag. J. Sci. **26**, 776 (1913).

[35] J. Serrin, in *Fluid Dynamics I/Strömungsmechanik I* (Springer, Berlin, 1959), pp. 125–263.

[36] K. Ho, D. Yang, and J. Wu, J. Eng. Thermophys. **9**, 10 (1988).

[37] J.-Z. Wu, H.-Y. Ma, and M.-D. Zhou, *Vorticity and Vortex Dynamics* (Springer Science & Business Media, Berlin, 2007).

[38] W. J. M. Rankine, Philos. Trans. R. Soc. London **160**, 277 (1870).

[39] P. Rankine, J. Ec. Polytech. (Paris) **57**, 3 (1887).

[40] M. D. Salas, Shock Waves **16**, 477 (2007).

[41] R. Courant and K. O. Friedrichs, *Supersonic Flow and Shock Waves*, Vol. 21 (Springer Science & Business Media, Berlin, 1999).

[42] R. Von Mises, H. Geiringer, and G. S. S. Ludford, *Mathematical Theory of Compressible Fluid Flow* (Courier Corporation, North Chelmsford, MA, 2004).

[43] S. E. Guarini, R. D. Moser, K. Shariff, and A. Wray, J. Fluid Mech. **414**, 1 (2000).

[44] S. Pirozzoli, F. Grasso, and T. Gatski, Phys. Fluids **16**, 530 (2004).

[45] H. Hornung and M. Robinson, J. Fluid Mech. **123**, 155 (1982).

[46] C. A. Mouton and H. G. Hornung, Phys. Fluids **20**, 541 (2008).

[47] D. J. Azevedo and C. S. Liu, AIAA J. **31**, 83 (1993).

[48] N. J. Wilkinson, M. A. Alam, J. M. Clayton, R. Evans, H. M. Fretwell, and S. G. Usmar, Phys. Rev. Lett. **69**, 3535 (1992).

[49] Q. Xu, I. D. Sharp, C. W. Yuan, D. O. Yi, C. Y. Liao, A. M. Glaeser, A. M. Minor, J. W. Beeman, M. C. Ridgway, P. Kluth, J. W. Ager, D. C. Chrzan, and E. E. Haller, Phys. Rev. Lett. **97**, 155701 (2006).

[50] B. Hof, J. Westerweel, T. M. Schneider, and B. Eckhardt, Nature **443**, 59 (2006).

[51] G. Ben-Dov and J. Cohen, Phys. Rev. Lett. **98**, 064503 (2007).

[52] K. Avila, D. Moxey, A. de Lozar, M. Avila, D. Barkley, and B. Hof, Science **333**, 192 (2011).

[53] G. Lemoult, L. Shi, K. Avila, S. V. Jalikop, M. Avila, and B. Hof, Nat. Phys. **12**, 254 (2016)

[54] Muellerand E. J., Phys. Rev. A **66**, 063603 (2002).

[55] D. Diakonov, L. M. Jensen, C. J. Pethick, and H. Smith, Phys. Rev. A **66**, 013604 (2002).

[56] O. Morsch and M. Oberthaler, Rev. Mod. Phys. **78**, 179 (2006).

[57] S. Eckel, J. G. Lee, F. Jendrzejewski, N. Murray, C. W. Clark, C. J. Lobb, W. D. Phillips, M. Edwards, and G. K. Campbell, Nature **506**, 200 (2014).

[58] X. Li, D. Fu, and Y. Ma, Sci. China, Ser. G: Phys. Mech. Astron. **51**, 699 (2008).

[59] Y. S. Zhang, W. T. Bi, F. Hussain, X. L. Li, and Z. S. She, Phys. Rev. Lett. **109**, 054502 (2012).

[60] Y.-C. Hu, W.-T. Bi, S.-Y. Li, and Z.-S. She, Sci. China: Phys., Mech. Astron. **60**, 124711 (2017).

[61] Y.-C. Hu, W.-F. Zhou, G. Wang, Y.-G. Yang, and Z.-G. Tang, Phys. Fluids **32**, 113601 (2020).

[62] S. Gottlieb and C.-W. Shu, Math. Comput. **67**, 73 (1998).